Biochemical and Biophysical Research Communications 430 (2013) 541–546

Contents lists available at SciVerse ScienceDirect

Biochemical and Biophysical Research Communications

journal homepage: www.elsevier.com/locate/ybbrc

# Solution structure and dynamics of C-terminal regulatory domain of *Vibrio vulnificus* extracellular metalloprotease

Ji-Hye Yun [a], Heeyoun Kim [a], Jung Eun Park [b], Jung Sup Lee [b,*], Weontae Lee [a,*]

[a] Department of Biochemistry, College of Life Science and Biotechnology, Yonsei University, Seoul 120-749, Republic of Korea
[b] Department of Biotechnology, College of Natural Sciences, Chosun University, Gwangju 501-759, Republic of Korea

ARTICLE INFO

*Article history:*
Received 19 November 2012
Available online 7 December 2012

*Keywords:*
*Vibrio* extracellular metalloprotease (vEP)
NMR spectroscopy
Wound infection
Septicemia
Solution structure
Fluorescence

ABSTRACT

An extracellular metalloprotease (vEP) secreted by *Vibrio vulnificus* ATCC29307 is a 45-kDa proteolytic enzyme that has prothrombin activation and fibrinolytic activities during bacterial infection. The action of vEP could result in clotting that could serve to protect the bacteria from the host defense machinery. Very recently, we showed that the C-terminal propeptide (C-ter100), which is unique to vEP, is involved in regulation of vEP activity. To understand the structural basis of this function of vEP C-ter100, we have determined the solution structure and backbone dynamics using multidimensional nuclear magnetic resonance spectroscopy. The solution structure shows that vEP C-ter100 is composed of eight anti-parallel β-strands with a unique fold that has a compact β-barrel formation which stabilized by hydrophobic and hydrogen bonding networks. Protein dynamics shows that the overall structure, including loops, is very rigid and stabilized. By structural database analysis, we found that vEP C-ter100 shares its topology with that of the collagen-binding domain of collagenase, despite low sequence homology between the two domains. Fluorescence assay reveals that vEP C-ter100 interacts strongly with iron ($Fe^{3+}$). These findings suggest that vEP protease might recruit substrate molecules, such as collagen, by binding at C-ter100 and that vEP participates in iron uptake from iron-withholding proteins of the host cell during infection.


## 1. Introduction

Extracellular proteases have been studied as important enzymes due to their implication in pathogenesis. *Vibrio vulnificus*, which causes wound infection and septicemia, is a Gram-negative halophilic marine bacterium [1,2]. *V. vulnificus* secretes a metalloprotease (vEP) that is composed of a signal peptide, N-terminal propeptide (nPP), C-terminal propeptide (C-ter100), and catalytic domains [3–5]. The signal sequence targets the enzyme for secretion, and the nPP functions as an intramolecular chaperone that is required for the folding of the polypeptide, and also acts as an inhibitor, preventing premature activation of the enzyme. The proenzyme is activated to a 45-kDa mature enzyme (vEP-45) after release of the nPP region. vEP-45 can be further autoprocessed to a 34-kDa form (vEP-34) with the loss of the C-terminal propeptide (C-ter100). vEP has many biological functions, including prothrombin activation and fibrinolysis [3] and it employs a broad spectrum of substrates. In our previous report, we showed that vEP-45 and vEP-34 have similar protease activities. However, vEP-34 shows lower catalytic efficiency than vEP-45 when it cleaves protein substrates that are associated with blood clotting, such as prothombin, plasminogen, fibrinogen, and factor Xa, as well as with plasma proteins not associated with blood clotting, such as albumin and γ-globulin [3,6]. We have suggested that vEP C-ter100 could play an important role in substrate binding prior to cleavage [3,6]. Although it is essential to deduce the structure of vEP to elucidate the mechanism underlying its proteolytic activity, no detailed structural information has been reported.

Here we present the high-resolution solution structure and dynamic profile of vEP C-ter100 generated by nuclear magnetic resonance (NMR) spectroscopy. The solution structure demonstrated that vEP C-ter100 has a unique β-barrel fold, consisting of eight anti-parallel β-strands, and that it shares molecular topology with the collagen-binding domain of collagenase. Structural information suggests that in the mature, active vEP, vEP C-ter100 might interacts with collagen. In addition, we propose that vEP C-ter100 could function in iron ion uptake, based on fluorescence data and NMR titration

*Abbreviations:* vEP, *Vibrio vulnificus* extracellular metalloprotease; NMR, nuclear magnetic resonance; C-ter100, C-terminal propeptide; NOESY, nuclear Overhauser effect spectroscopy; HCCH, hydrogen–carbon–carbon–hydrogen; TOCSY, total correlated spectroscopy; 3D, three-dimensional; PDB, protein data bank.

* Corresponding authors. Addresses: Department of Biotechnology, College of Natural Sciences, Chosun University, 375 Seosuk-dong Dong-gu, Gwangju 501-759, Republic of Korea. Fax: 82 62 233 6851 (J.S. Lee), Department of Biochemistry, College of Life Science and Biotechnology, Yonsei University, 134 Shinchon-Dong Seodaemoon-Gu, Seoul 120-749, Republic of Korea. Fax: +82 2 363 2706 (W. Lee).
*E-mail addresses:* jsplee@mail.chosun.ac.kr (J.S. Lee), wlee@spin.yonsei.ac.kr (W. Lee).

0006-291X/$ - see front matter © 2012 Elsevier Inc. All rights reserved.
http://dx.doi.org/10.1016/j.bbrc.2012.11.117

experiments. These data should advance our understanding of the proteolytic function of vEP in terms of the regulatory role of vEP C-ter100, and may be directly applicable to the study of structure-function relationships in the metalloprotease family of proteins.

## 2. Materials and methods

### 2.1. NMR sample preparation

Sequence encoding the vEP C-ter100 was amplified from *V. vulnificus* ATCC 29307 chromosomal DNA and cloned into the *Bam*HI/*Xho*I site of plasmid pET32a (Novagen, Madison, WI) containing the TEV protease cleavage site (ENLYFQG). Isotopically labeled protein was overexpressed in M9 minimal media overnight at 25 °C in the presence of 1 mM IPTG and [U–$^{13}$C] glucose and/or $^{15}NH_4Cl$ as carbon and nitrogen sources, respectively. The molecular weight of the purified protein was determined by reference to the standard proteins albumin (66 kDa), carbonic anhydrase (29 kDa), cytochrome c (12.4 kDa), and aprotinin (6.5 kDa). Final NMR samples were concentrated to 0.6 mM in NMR buffer (20 mM HEPES, pH 7.0, 100 mM NaCl, 0.01% $NaN_3$) using an Amicon Ultra-15 concentration device (Millipore, Billerica, MA) and transferred to a 5-mm symmetrical microcell (Shigemi, Allison Park, PA).

### 2.2. NMR spectroscopy and structure determination

All NMR data were collected at 298 K on Bruker DRX500 and DRX900 spectrometers with triple-resonance probes equipped with triple-axis gradient coils. Sequential resonance assignment was executed by $^{1}$H–$^{15}$N heteronuclear single quantum coherence [7], three-dimensional (3D) HNCACB, CBCACONH, HBHACONH, and HNCA experiments [7–12], and confirmed by sequential NOEs derived from $^{15}$N-edited nuclear Overhauser effect spectroscopy (NOESY) [13,14] with a mixing time of 150 ms. Side chain assignments were completed using 3D hydrogen–carbon–carbon–hydrogen total correlation spectroscopy (HCCH–TOCSY), (H)CC(CO)NH, and HCC(CO)NH [15,16]. Torsion angle ($\Psi$, $\Phi$) values from torsion angle likelihood obtained from shift and sequence similarity (TALOS) analysis were used during structure calculation as CYANA restraints. $^{15}$N-edited NOESY ($\tau_m$ = 150 ms) and $^{13}$C-edited NOESY ($\tau_m$ = 150 ms) spectra were obtained using a 900-MHz Bruker DRX 900 spectrometer equipped with a CryoProbe™ at 298 K. Structure calculations were performed using the CYANA 2.2.5 program with Linux cluster. The 20 lowest-energy structures from 100 simulated annealing conformers of 10,000 torsion angle dynamics steps were selected for further analysis. Final structures were refined using the CNS program and analyzed with PROCHECK [17], PyMOL, and MOLMOL [18] software. The data from resonance assignments were deposited in the Biological Magnetic Resonance Bank under accession code 18338. The atomic coordinates of the 20 final structures, together with the energy-minimized average structure of vEP C-ter100, were deposited in the Protein Data Bank (PDB) under accession code 2luw.

The following servers were used for sequence and structural analyses: BLAST (http://blast.ncbi.nlm.nih.gov/Blast.cgi), ClustalW2 (http://www.ebi.ac.uk/Tools/clustalw2), DALI (http://ekhidna.biocenter.helsinki.fi/dali-server), and SCOP (http://scop.mrc-lmb.cam.ac.uk/scop).

### 2.3. Fluorescence experiments

All experiments were performed at 298 K using an RF-530 PC spectrofluorophotometer (Shimadzu, Kyoto, Japan). The vEP C-ter100 (10 μM) was prepared in 10 mM HEPES (pH 7.0) containing 100 mM NaCl and 2 mM dithiothreitol. Three metal ions ($FeCl_3$, $MnCl_2$, and $LiCl_2$) were dissolved in buffer to a final concentration of 1 mM for titration experiments. The sample was contained in a 1 mL thermostated cuvette and fluorescence experiments were performed in the ranges of 280 nm and 200–500 nm wavelength. $K_d$ values were calculated using the following equation: $\log(F_0 - F/F) = \log 1/K_d + n\log[\text{inhibitor}]$.

### 2.4. Backbone dynamics

Backbone dynamics experiments for vEP C-ter100 were performed as previously reported [19]. Longitudinal ($T_1$) and transverse ($T_2$) relaxation data for the backbone amide $^{15}$N nuclei were recorded as 2048 × 128 data sets with 64 scans per point, using 3 s of relaxation recovery time. Seven relaxation times were used for $T_1$ (50, 150, 300, 500, 700, 1000, and 1500 ms) and $T_2$ (20, 40, 60, 80, 100, 120, and 140 ms) for recording with delays. For estimation of noise levels, duplicate spectra were recorded for values of $T_1$ = 150 ms and $T_2$ = 40 ms. The steady-state heteronuclear NOE (XNOE) [19,20] experiment was obtained as 2048 × 128 data sets using a relaxation delay of 3 s. Both unsaturated and saturated XNOE spectra were acquired by interleaving pulse sequences and were separately processed using the XWINNMR program. $R_1$, $R_2$, and XNOE data were processed and analyzed with the NMR Pipe and Sparky programs. Peak heights and signal-to-noise values of each $R_1$ and $R_2$ spectrum were used to determine both $T_1$ and $T_2$ decay rates, using an exponential function with the Curve Fit program from Arthur G. Palmer (http://cpmcnet.columbia.edu/dept/gsas/biochem/labs/palmer/software/curvefit.html). The heteronuclear NOE values were determined by the ratio of the peak heights from the unsaturated and saturated XNOE spectra and error values were calculated using the equation $\sigma_{NOE}/NOE = [(\sigma I_{sat}/I_{sat})^2 + (\sigma I_{unsat}/I_{unsat})^2]^{1/2}$, where $I_{sat}$ and $I_{unsat}$ represent the cross-peak intensities and $\sigma I_{sat}$ and $\sigma I_{unsat}$ represent the root mean square noise value of the background in proton-saturated and -unsaturated spectra. The $\tau_m$ and rotational diffusion tensor were determined from the $R_2/R_1$ ratio using the Diffusion program, and the inertia tensor was calculated from the PDB coordinates of vEP C-ter100 using the Pdbinertia program. The generalized order parameter ($S^2$) and chemical exchange term ($R_{ex}$) were determined with the Fastmodelfree program using an axially symmetric diffusion tensor.

## 3. Results and discussion

### 3.1. Structure determination and solution structure of vEP C-ter100

Gel-filtration chromatography shows that vEP C-ter100 is a monomer [21]. All backbone and side-chain resonances were completely assigned using data from HNCA, CBCACONH, HNCACB, HCCH–TOCSY, and $^{15}$N-edited NOESY experiments. Secondary structures were determined by data from the chemical shift indices, NOEs, and $^{3}J_{HN\alpha}$ coupling constants. A total of 1698 unambiquous NOEs (845 short-range ($|i-j| = 1$), 93 medium-range ($1 < |i-j| < 5$), 760 long-range ($|i-j| \geqslant 5$) NOE constraints), 29 backbone hydrogen bonds, and 103 dihedral angle restraints from NMR experiments were derived for structure determination. The 20 lowest-energy structures from 100 calculated conformers were selected for detailed analysis. The structural statistics associated with the 20 final structures are listed in Table 1. The final 20 structures were well converged with root mean square deviation (RMSD) values of 0.35 ± 0.05 and 0.79 ± 0.09 Å for backbone and all heavy atoms, respectively (Fig. 1A). The vEP C-ter100 is composed of eight anti-parallel β-strands (residues of β1(518–525), β2(527–536), β3(539–546), β4(553–559), β5(569–571), β6(578–585), β7(588–597) and β8(600–606)) (Fig. 1B). The structure of vEP C-ter100 is relatively rigid and a central β-barrel is well

**Table 1**
NMR structural statistics.

| Distant restraints in the structure calculation | |
|---|---|
| All | 1698 |
| Short range {$\|i-j\|=1$} | 845 |
| Medium range {$2 \leqslant \|i-j\| \leqslant 5$} | 93 |
| Long range {$\|i-j\|>5$} | 760 |
| Hydrogen bond restraints[a] | 29 |
| Dihedral angle restraints | |
| All | 103 |
| $\Phi$ | 51 |
| $\Psi$ | 52 |
| Residual violations | |
| CYANA target functions, Å | 11.3 ± 0.5 |
| NOE upper distance constrain violation | |
| Ave, Å (<0.1 A) | 0.71 ± 0.02 |
| Dihedral angle constrain violations | |
| Ave,° (<5°) | 17.09 ± 0.74 |
| Vander Waals violations | |
| Ave, Å (<0.2 A) | 0.31 ± 0.03 |
| RMS deviations from the average coordinate[b], Å | |
| Backbone atoms | 0.35 ± 0.05 |
| All heavy atoms | 0.79 ± 0.09 |
| Ramachandran statistics,% of all residues | |
| Residues in most favored regions | 72.9% |
| Residues in additional allowed regions | 22.4% |
| Residues in generously allowed regions | 4.7% |
| Residues in disallowed allowed regions | 0% |

[a] Two restraints per one hydrogen bond.
[b] RMSD values for residues 510–609 a.a.

defined, including most of loops (Fig. 1A). The molecular topology shows that vEP C-ter100 has a unique fold with an eight-stranded anti-parallel β-barrel (Fig. 1C). The structure is composed of three pleated sheets connected by linkers β1–β8, β3–β6 and β2–β7–β4–β5. Interestingly, the first strand, β1, interacts with β8, forming a small anti-parallel β-sheet, which serves as a key strand to integrate the three β-sheets (Fig. 1B). All β strands are involved in an extensive hydrogen-bonding network, which is a major stabilization force in vEP C-ter100. A number of hydrophobic residues are found on the hydrophobic patch of the protein, preventing vEP C-ter100 flexibility. The surface charge distribution on the protein shows a cluster of positively-charged residues (mainly Lys), which allow electrostatic interactions with putative vEP C-ter100 ligands/receptor molecules (Fig. 1D).

### 3.2. Backbone dynamics of vEP C-ter100

The experimental $T_1$, $T_2$, and steady-state $^{15}N$–{$^1H$} heteronuclear NOE (XNO4E) data are summarized in Fig. 2. The average values of $R_1$ and $R_2$ were determined to be 0.66 $s^{-1}$ (Fig. 2A) and 25.13 $s^{-1}$ (Fig. 2B), respectively. The $^{15}N$–{$^1H$} heteronuclear NOEs for most regions were 0.8–1.0. The profile of vEP C-ter100 backbone dynamics shows that the overall structure, including loops, is very rigid (Fig. 3C). However, residues in the β3 region exhibit smaller $^{15}N$–{$^1H$} steady-state heteronuclear NOEs and order parameters, as well as longer internal correlation times, than those of residues in the structured regions, implying that β3 could be intrinsically dynamic or involved in putative ligand/receptor binding (Fig. 2A–C). The overall rotational correlation time ($\tau_m$) determined from the $R_1$, $R_2$ and XNOE values and NMR structure was calculated to be 12.82 ns. The calculated order parameters ($S^2$) of most residues were in the range 0.9–1.0, showing that vEP C-ter100 is highly ordered due to its compact β-barrel structure (Fig. 2D). The effective correlation time for internal motions, $\tau_e$,

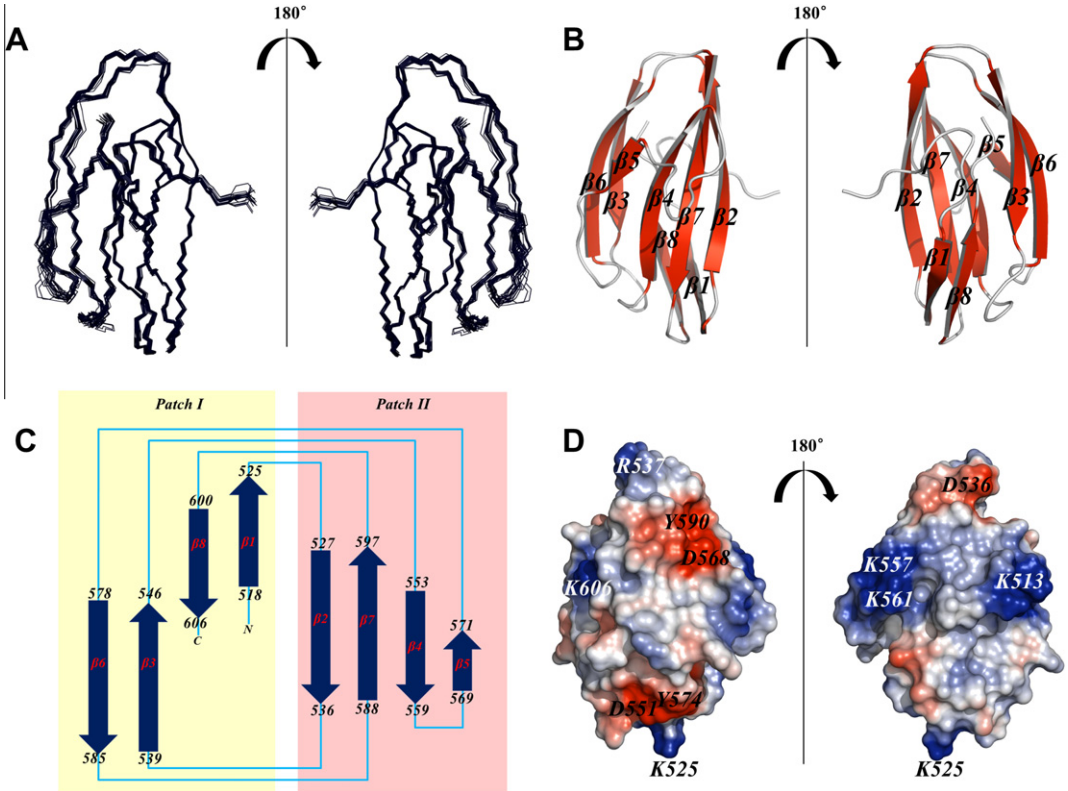


**Fig. 1.** NMR structures of vEP C-ter100. (A) Backbone superposition of the final 20 structures over the energy-minimized average structure. The structures were overlapped on the basis of the backbone atoms $C_\alpha$, CO, and NH. (B) Solution structure of vEP C-ter100 represented by ribbon diagram. The structure was visualized using the program Pymol. Eight β strands are represented. (C) Schematic diagram of the molecular topology of vEP C-ter100. β-Strands are shown as arrows with numbers. (D) Electrostatic potential of the surface of vEP C-ter100. The positively and negatively charged surfaces are shown in blue and red, respectively. The structure was generated using the APBS [27] program. (For interpretation of colors in this figure legend, the reader is referred to the web version of this article.)

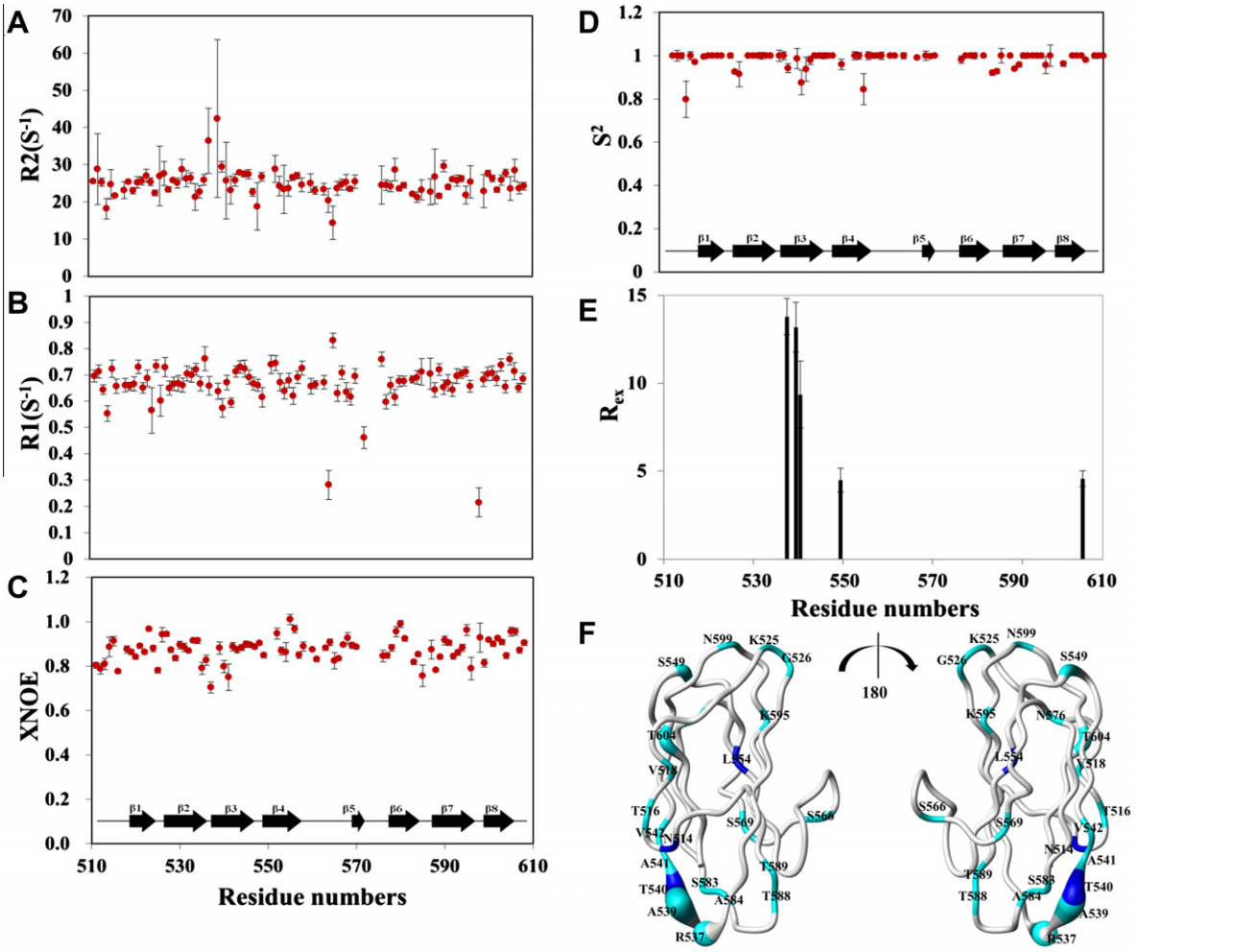


**Fig. 2.** Data from vEP C-ter100 backbone dynamics experiments. (A) Measured values of spin–lattice relaxation rate ($R_1[S^{-1}]$) are shown. (B) Values of spin–spin relaxation rate ($R_2[S^{-1}]$) are displayed. (C) Heteronuclear NOE (XNOE) data are shown. (D, E) Optimized values of the generalized order parameter ($S^2$) (D) and exchange parameters ($R_{ex}$) (E) are shown. (F) Dynamic regions in the structure of vEP C-ter100 are shown in blue. (For interpretation of colors in this figure legend, the reader is referred to the web version of this article.)

and chemical exchange of the β3 region support the dynamics profile (Fig. 2E).

In overall structure, residues in β3 exhibit smaller XNOEs, and longer internal correlation times than residues in the other regions, indicating that β3 is intrinsically dynamic, although vEP C-ter100 forms a relatively compact structure (Fig. 2F).

### 3.3. Fluorescence analysis on metal ion binding

It is known that most metalloproteases interact with metal ion for their activities. Previous reports suggest that the vEP protease facilitates iron uptake from iron-withholding protein [22–24] and binding of the iron ion affects vEP production [25]. We investigated interactions between metal ions and vEP C-ter100. Data from fluoresence experiments shows that vEP C-ter100 interacts strongly with $Fe^{3+}$ (Fig. 3A), but has no interaction with $Mg^{2+}$ (Fig. 3B) and very weak interaction with $Li^{2+}$ (Fig. 3C). Dissociation constants ($K_d$) were determined to be $2.587 \times 10^{-8}$ M ($Fe^{3+}$) and $2.8 \times 10^{-3}$ M ($Li^{2+}$), respectively. NMR titration experiments provide residue-specific information for the metal ion interaction. Upon $Fe^{3+}$ titration, four residues of vEP C-ter100 disappeared and several residues experienced chemical shift perturbation (Fig. 3D). In particular, tyrosine residues Y555, Y572, Y574, and Y597 were involved in the metal interaction, as shown in Fig. 3D and E. Because Y597 is far from the other three residues, the observed perturbation of Y597 could originate from changes in local environments upon iron binding.

### 3.4. Functional implications of vEP C-ter100

Both primary sequence analysis and NMR structure were used to derive functional information for vEP C-ter100 using the BLAST, DALI, and SCOP servers. BLAST analysis did not identify any protein structures having sequence homology with vEP C-ter100. However, DALI and SCOP searches using the solution structure of vEP C-ter100 suggested that the molecular topology of vEP C-ter100 is shared with that of the collagen-binding domain of collagenase (PDB: 1NQJ), with root-mean-square deviation = 3.4 Å of root mean square although they share a very low level of sequence identity. Maxium *Z*-score derived from DALI server is 3.2. This result suggests that vEP C-ter100 and the collagen-binding domain of collagenase might serve similar functions in proteolytic activity. Our preliminary data indicates that C-terminal truncated vEP (vEP-34) exhibits approximately 60% lower efficiency than mature vEP-45 in cleaving insoluble collagen IV (data not shown). This suggests that vEP C-ter100 could directly bind to collagen or other

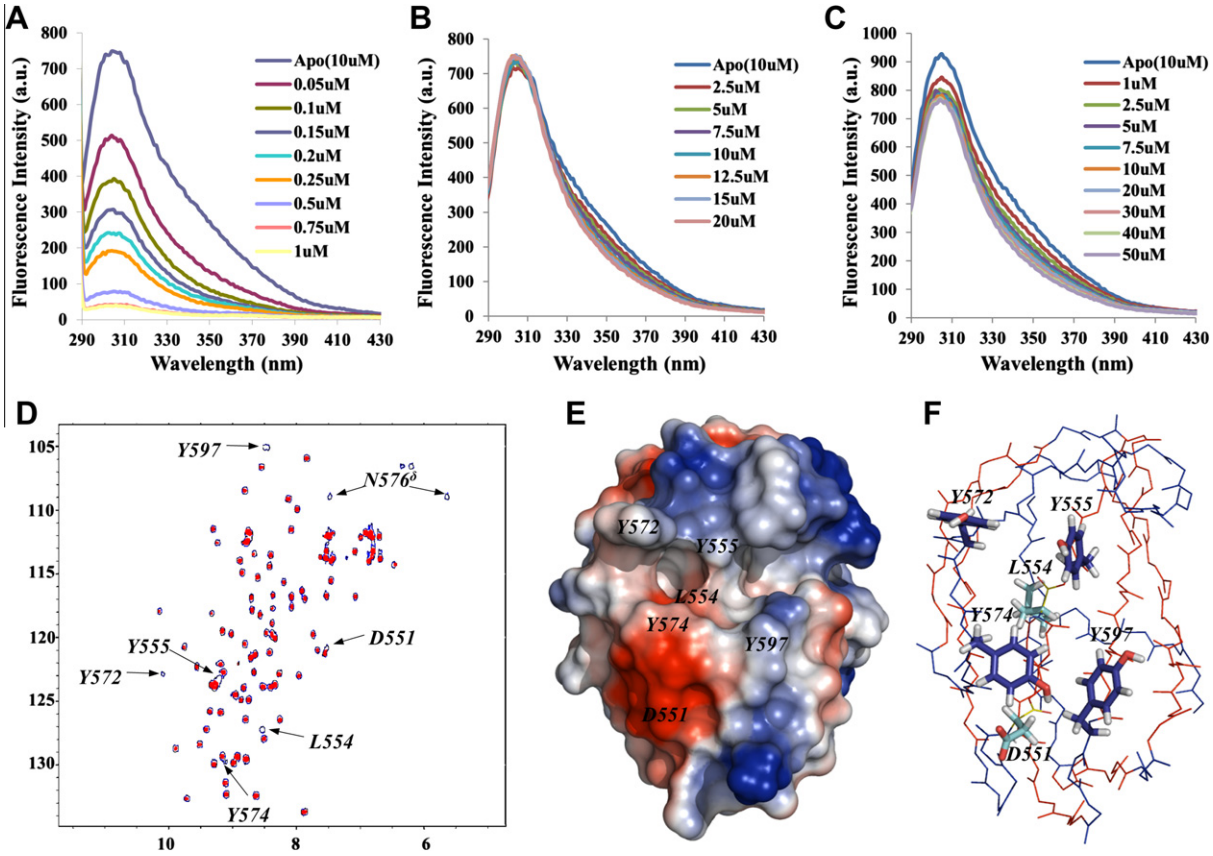


**Fig. 3.** The vEP C-ter100 interacts with iron ion through four tyrosine residues. Fluorescence assay of vEP C-ter100 in the presence of (A) $Fe^{3+}$, (B) $Mn^{2+}$, and (C) $Li^{2+}$ ions. Samples were excited at 280 nm and emission spectra were recorded for light-scattering effects from 290 to 430 nm. All assays were performed in 20 mM HEPES, pH 7.5, and 100 mM NaCl using 10 μM vEP and increasing concentrations of metal ions. Ion concentrations are indicated by different colors. *X* and *Y* axis of the spectra indicates the wavelength (nm) and fluorescence intensity (a.u.). (D) NMR titration spectra in the absence (blue) and presence (red) of iron ion. Six residues (D551, L554, Y555, Y572, Y574 and Y597), indicated by arrows, disappeared completely as a result of the iron interaction. The other residues overlap well. (E) Iron-binding site is represented in surface charge model. The six residues that disappeared during NMR titration (D551, L554, Y555, Y572, Y574, and Y597) are located in close proximity to each other and a binding pocket has formed around them. (F) The putative iron-binding site in vEP C-ter100 suggested by NMR titration are shown in stick representation and labeled. The side chain orientations of four tyrosine residues (Y555, Y572, Y574 and Y597) nearly located on the surface are marked by dark blue. L554 located on hydrophobic pore and D551 located on negatively charged surface are also affected on iron-binding and marked by light blue. (For interpretation of colors in this figure legend, the reader is referred to the web version of this article.)

insoluble protein substrates, during the vEP cleavage reaction. Previous studies have also demonstrated that vEP C-ter100 is essential for cleaving insoluble proteins, such as collagen, fibrin and elastin [6,26].

Because C-terminal propeptide domains are not frequently found in the mature forms of metalloproteases and serine proteases, vEP is unique in having a C-terminal propeptide domain that is essential to efficient proteolysis of insoluble protein substrates and erythrocyte membranes. The solution structure of vEP C-ter100 shows that the C-terminal itself forms a compact three-dimensional structure with an iron-binding site, providing information on the structure of potential binding partners. Iron binding to vEP C-ter100 might be important in vEP function as well. Our hypothesis proposes that vEP C-ter100 activates prothrombin to take up iron in the blood coagulation pathway. Since iron binding residues are highly conserved in metalloproteases of many other bacterial species, our data should be applicable in studying other metal-binding proteins.

## Acknowledgments

This work was supported by the Korea Research Foundation (KRF) grant funded by the Korea government (MEST) (No. 2010-0026307).

## References

[1] S.R. Chiang, Y.C. Chuang, *Vibrio vulnificus* infection: clinical manifestations, pathogenesis and antimicrobial therapy, J. Microbiol. Immunol. Infect. 36 (2003) 81–88.
[2] O. Ulusarac, E. Carter, Varied clinical presentations of *Vibrio vulnificus* infections: a report of four unusual cases and review of the literature, S. Med. J. 97 (2004) 163–168.
[3] A.K. Chang, J.W. Park, E.H. Lee, J.S. Lee, The N-terminal propeptide of *Vibrio vulnificus* extracellular metalloprotease is both an inhibitor of and a substrate for the enzyme, J. Bacteriol. 189 (2007) 6832–6838.
[4] J.Y. Kwon, A.K. Chang, J.E. Park, S.Y. Shin, S.M. Yoon, J.S. Lee, *Vibrio* extracellular protease with prothrombin activation and fibrinolytic activities, Int. J. Mol. Med. 19 (2007) 157–163.
[5] H.Y. Kim, A.K. Chang, J.E. Park, I.S. Park, S.M. Yoon, J.S. Lee, Procaspase-3 activation by a metalloprotease secreted from *Vibrio vulnificus*, Int. J. Mol. Med. 20 (2007) 591–595.
[6] S. Miyoshi, H. Wakae, K. Tomochika, S. Shinoda, Functional domains of a zinc metalloprotease from *Vibrio vulnificus*, J. Bacteriol. 179 (1997) 7606–7609.
[7] G.W. Vuister, A. Bax, Quantitative J correlation: a new approach for measuring homonuclear three bond J(HNHa) coupling constants in 15N-enriched proteins, J. Am. Chem. Soc. 115 (1993) 7772–7777.
[8] S. Grzesiek, A. Bax, Improved 3D Triple-resonance NMR techniques applied to a 31-kDa protein, J. Magn. Reson. 96 (1992) 432–440.
[9] J. Stonehouse, R.T. Clowes, G.L. Shaw, J. Keeler, E.D. Laue, Minimisation of sensitivity losses due to the use of gradient pulses in triple-resonance NMR of proteins, J. Biomol. NMR 5 (1995) 226–232.
[10] D.R. Muhandiram, L.E. Kay, Gradient-enhanced triple-resonance three-dimensional NMR experiments with improved sensitivity, J. Magn. Reson. 103 (1994) 203–216.

[11] M. Ikura, L.E. Kay, A. Bax, A novel approach for sequential assignment of 1H, 13C, and 15N spectra of proteins: heteronuclear triple-resonance three-dimensional NMR spectroscopy application to calmodulin, Biochemistry 29 (1990) 4659–4667.
[12] A. Grzesiek, A. Bax, The origin and removal of artifacts in 3d HCACO spectra of proteins uniformly enriched with $^{13}C$, J. Magn. Reson. 102 (1993) 103–106.
[13] M. Piotto, V. Saudek, V. Sklenar, Gradient-tailored excitation for single-quantum NMR spectroscopy of aqueous solutions, FEBS Lett. 2 (1992) 661–665.
[14] A.L. Davis, J. Keeler, E.D. Laue, D. Moskau, Experiments for recording pureabsorption heteronuclear correlation spectra using pulsed field gradients, J. Magn. Reson. 98 (1992) 207–216.
[15] L.E. Kay, G.Y. Xu, A.U. Singer, D.R. Muhandiram, J.D. Forman-Kay, A gradient-enhanced HCCH–TOCSY experiment for recording sidechain 1H and 13C correlations in H2O samples of proteins, J. Magn. Reson. 101 (1993) 333–337.
[16] A. Bax, D.G. Davis, MLEV-17 based 2D homonuclear magnetization transfer spectroscopy, J. Magn. Reson. 65 (1985) 355–360.
[17] R.A. Laskowski, J.A. Rullmannn, M.W. MacArthur, R. Kaptein, J.M. Thornton, AQUA and PROCHECK-NMR: programs for checking the quality of protein structures solved by NMR, J. Biomol. NMR 8 (1996) 477–486.
[18] .R. Koradi, M. Billeter, K. Wuthrich, MOLMOL: a program for display and analysis of macromolecular structures, J. Mol. Graphics 14 (1996) 51–55. 29–32.
[19] N.A. Farrow, R. Muhandiram, A.U. Singer, S.M. Pascal, C.M. Kay, G. Gish, S.E. Shoelson, T. Pawson, J.D. Forman-Kay, L.E. Kay, Backbone dynamics of a free and phosphopeptide-complexed Src homology 2 domain studied by 15N NMR relaxation, Biochemistry 33 (1994) 5984–6003.
[20] S. Grzesiek, A. Bax, The importance of not saturating HzO in protein NMR application to sensitivity enhancement and NOE measurements, J. Am. Chem. Soc. 115 (1993) 12593–12594.
[21] J.H. Yun, H. Kim, J.E. Park, H.K. Cheong, C. Cheong, J.S. Lee, W. Lee, $^{1}H$, $^{15}N$ and $^{13}C$ backbone assignments and secondary structures of C-ter100 domain of *Vibrio* extracellular metalloprotease derived from *Vibrio vulnificus*, Bull. Korean Chem. Soc. 33 (2012) 3248–3252.
[22] Y. Nishina, S. Miyoshi, A. Nagase, S. Shinoda, Significant role of an exocellular protease in utilization of heme by *Vibrio vulnificus*, Infect. Immunol. 60 (1992) 2128–2132.
[23] J.G. Morris, A.C. Wright, L.M. Simpson, P.K. Wood, D.E. Johnson, J.D. Oliver, Virulence of *Vibrio vulnificus*: association with utilization of transferrin-bound iron, and lack of correlation with levels of cytotoxin or protease production, FEMS Microbiol. Lett. 40 (1987) 55–59.
[24] A.M. Starks, T.R. Schoeb, M.L. Tamplin, S. Parveen, T.J. Doyle, P.E. Bomeisl, G.M. Escudero, P.A. Gulig, Pathogenesis of infection by clinical and environmental strains of *Vibrio vulnificus* in iron-dextran-treated mice, Infect. Immunol. 68 (2000) 5785–5793.
[25] C.M. Kim, S.C. Kim, S.H. Shin, Iron-mediated regulation of metalloprotease VvpE production in *Vibrio vulnificus*, New Microbiol. 35 (2012) 481–486.
[26] A.K. Chang, H.Y. Kim, J.E. Park, P. Acharya, I.S. Park, S.M. Yoon, H.J. You, K.S. Hahm, J.K. Park, J.S. Lee, *Vibrio vulnificus* secretes a broad-specificity metalloprotease capable of interfering with blood homeostasis through prothrombin activation and fibrinolysis, J. Bacteriol. 187 (2005) 6909–6916.
[27] N.A. Baker, D. Sept, S. Joseph, M.J. Holst, J.A. McCammon, Electrostatics of nanosystems: application to microtubules and the ribosome, Proc. Natl. Acad. Sci. 98 (2001) 10037–10041.